Dust and Recent Star Formation in the Core of NGC5253. ¹

Daniela Calzetti

Space Telescope Science Institute, 3700 San Martin Dr., Baltimore, MD 21218, USA; e-mail: calzetti@stsci.edu

Gerhardt R. Meurer
Dept. of Physics and Astronomy, The Johns Hopkins University

Ralph C. Bohlin Space Telescope Science Institute

Donald R. Garnett
Dept. of Astronomy, University of Minnesota

Anne L. Kinney and Claus Leitherer Space Telescope Science Institute

and

Thaisa Storchi-Bergmann Instituto de Fisica, Universidade Federal Rio Grande do Sul

ABSTRACT

Ultraviolet and optical narrow and broad band images of NGC5253 obtained with the Hubble Space Telescope Wide Field and Planetary Camera 2 are used to derive the properties of the dust distribution and the recent star formation history of this metal-poor dwarf galaxy. Corrections for the effects of dust are important in the center of NGC5253: dust reddening is markedly inhomogeneous across the galaxy's central 20" region. One of the most obscured regions coincides with the region of highest star formation activity in the galaxy; clouds of more than 9 magnitudes of optical depth at V enshroud a 2.5 Myr old stellar cluster in this area. The ages of the bright clusters in the center of the galaxy are anti-correlated with the amount of dust obscuration the cluster suffers. This result agrees with the expectation that young stellar associations are located in heavily obscured regions, but after only 2–3 Myr they remove/emerge from the parental dust cloud and become almost extinction-free. On average, the

¹Based on observations obtained with the NASA/ESA *Hubble Space Telescope* at the Space Telescope Science Institute, which is operated by the Association of Universities for Research in Astronomy, Inc., under NASA contract NAS5-26555.

continuum emission of the diffuse stellar population is about a factor two less reddened than the ionized gas emission, a behavior typical of starburst galaxies (Calzetti et al. 1994). In the case of NGC5253, this difference originates from the larger scale length of the star distribution relative to the ionized gas: the half light radius of the UV-bright stars is about twice as large as the half light radius of the ionized gas emission.

Star formation has been active at least over the past 100 Myr in the central 20" of the galaxy, as indicated by the age distribution of both the blue diffuse stellar population and the bright stellar clusters. The star formation episodes may have been discrete in time, or almost continuous but variable in intensity and spatial extension. The current peak of the star formation is located in a 6" region, more spatially concentrated than the star formation averaged over the past 100 Myr. Its average star formation intensity is 10^{-5} – 10^{-4} M $_{\odot}$ /yr/pc² for a 0.1–100 M $_{\odot}$ Salpeter IMF, a factor 10 to 100 times larger than in the galaxy's central 20". This starburst region contains a stellar population \sim 5 Myr old and the two youngest (2.5 Myr and \sim 3–4 Myr, respectively) of the bright stellar clusters in the galaxy's center. The two clusters contribute between 20% and 65% of the ionizing photons in the starburst, a contribution between 1.3 and 4.3 times larger than the average over the central 20". This is expected if cluster formation is an important mode of star formation in the early phase of a starburst event. The mass of the 2.5 Myr old cluster may be as large as \sim 10⁶ M $_{\odot}$, making this one a Super-Star-Cluster candidate.

Subject headings: galaxies: starburst – galaxies: ISM – galaxies: photometry – ISM: dust, extinction

1. Introduction

Bursts of star formation play an important role in the framework of galaxy evolution. In the local Universe, more than half of the high-mass star formation comes from the nuclear region of galaxies (Gallego et al. 1995); within 10 Mpc of the Galaxy, 25% of the high-mass star formation is produced by less than a handful of starburst galaxies (Heckman 1997). At intermediate redshifts (z~0.3), the bulk of the excess faint blue galaxy counts may be due to a dwarf galaxy population experiencing sudden, high-efficiency and fast-evolving starbursts (e.g., Colless et al. 1994, Phillips & Driver 1995, Babul & Ferguson 1996). At higher redshifts (z~3), the recently discovered galaxy population (Steidel et al. 1996) has properties indicating a high-intensity starforming phase (e.g., Steidel et al. 1996, Giavalisco, Steidel & Macchetto 1996; see, also, Lowenthal et al. 1997). To the extent that the initial mass function (IMF) is independent of the environment (Massey et al. 1995; Moffat 1996; Stasínska & Leitherer 1996), a significant fraction of star formation in the universe appears to occur through high intensity episodes. Hence to understand galaxy evolution, and cosmic evolution, we must understand bursts of star formation.

Open questions about starbursts most relevant to cosmic evolution include the following. (1) How long do starbursts last? The answer, determines how important individual burst are in shaping the galaxy's stellar population; is a galaxy likely to undergo short-lived (1–10 Myr) bursts or long-lived (\gg 10 Myr) bursts? Bursts duration also has bearing on the problem of the relative number of burst and postburst systems (Norman 1991). (2) How does star formation spread within a galaxy? At issue is how starbursts are fueled (e.g. Shlosman 1992, Olson & Kwan 1990), and whether the energetic feedback of high mass star formation into the ISM inhibits or enhances star formation (Shull 1993, Chu & Kennicutt 1994, Heckman, Armus, & Miley 1990, Lehnert & Heckman 1996). Finally, (3) how much star formation is obscured or hidden from view? The impact of dust obscuration on optical and ultraviolet surveys of galaxies must be assessed in order to get a census of the actual star formation in the universe.

The best place to look for answers to these questions are the nearest starburst galaxies. The high spatial resolution and the high signal-to-noise multiwavelength information which can be obtained for these systems allow the detailed investigation of the starburst 'phenomenon'. NGC5253, a dwarf galaxy in the Centaurus Group at the distance of 4.1 Mpc (Sandage et al. 1994), is an excellent laboratory for this study. Although the outer regions of the galaxy have properties similar to a dwarf elliptical galaxy (Sersic, Carranza & Pastoriza 1972, Caldwell & Phillips 1989), star formation is active in its central 20" (the "core" hereafter), as characterized by a high surface brightness blue continuum and intense line emission (e.g., Storchi-Bergmann, Kinney & Challis 1995). The core hosts about a dozen blue stellar clusters as well as diffusely distributed high mass stars (Meurer et al. 1995). The peak intensity of star formation, as inferred from the distribution of the H α emission, is concentrated in a $\sim 6''$ region in the Northern part of the core (the "nucleus" hereafter). The most recent star formation episode is probably responsible for heating the gas which emits in the soft X-ray (Martin & Kennicutt 1995), as well as for the complex system of loops and filaments of ionized gas (Marlowe et al. 1995). The inhomogeneous structure and the intense star formation in the central region of NGC5253 has suggested a classification closer to an amorphous galaxy or a blue compact dwarf (Sandage & Brucato 1979, Meurer et al. 1994), rather than an elliptical.

An encounter with the spiral M83, located at a projected separation of only 130 kpc, about 1–2 Gyr ago has been suggested as the trigger of the star formation in NGC 5253 (Rogstad, Lockart & Wright 1974, van den Bergh 1980, Caldwell & Phillips 1989). However, the starburst in the nucleus has probably an age ≤ 10 Myr, as implied by the presence of Wolf-Rayet stars (Campbell, Terlevich & Melnick 1986, Walsh & Roy 1987, 1989, Schaerer et al. 1997), the small number of red supergiants (Campbell & Terlevich 1984), and the purely thermal component of the radio emission (Beck et al. 1996). NGC 5253 is chemically inhomogeneous, displaying a region of enhanced Nitrogen abundance (Walsh & Roy 1989, Kobulnicky et al. 1997) which indicate recent pollution from ejecta of massive stars. Radial inflow of peripheral HI gas has been suggested as a possible source of fuel for the current starburst (Kobulnicky & Skillman 1995, Turner, Beck & Hurt 1997).

NGC 5253 is also an ideal target for mapping the effects of dust on a starburst. The extinction is irregular in the core of the galaxy and the central region is traversed by a dust lane along the E-W direction, bisecting the galaxy along the minor axis (Walsh & Roy 1989). The nucleus of NGC5253 is very red above 2 μ m (Moorwood & Glass 1982), indicating presence of hot dust probably heated by an obscured nucleus (A_V=8-25 mag, Aitken et al. 1982, Roche et al. 1991, Telesco, Dressel, & Wolstencroft 1993). Despite the strength of the mid and far infrared emission, the reddening determined from the intense nuclear Balmer lines of NGC5253 is generally small, while the ultraviolet (UV) spectral energy distribution is redder than expected from a young, unextincted starburst (Gonzalez-Riestra, Rego, & Zamorano 1987, Kinney et al. 1993, Calzetti, Kinney & Storchi-Bergmann 1994, CKS94 hereafter).

The purpose of this paper is twofold. (1) Investigate the past 100 Myr or so of the star formation history of NGC5253. This timescale can be considered a sort of "boundary" between short-lived and long-lived bursts of star formation, because it is much longer than the typical lifetime of O and B stars (≈10 Myr). (2) Measure the impact of dust obscuration on the intrinsic properties of the galaxy. The galaxy's star formation history can be tackled via the age distribution of the stellar populations, which is derived from multiwavelength observations. Here the effects of reddening must be carefully measured, since dust reddening and stellar population ageing produce similar colors, and the spectral energy distribution of a young dusty stellar population may resemble that of an old dust-free population. The first part of the paper is thus devoted at solving the age/dust degeneracy by constraining reddening effects. The present dataset is composed of ultraviolet (UV) and optical narrow- and broad-band images of NGC5253 recently obtained with the Hubble Space Telescope Wide Field and Planetary Camera 2 (WFPC2). The WFPC2 offers the high spatial resolution necessary to isolate structures on the scale of HII complexes in nearby galaxies. The multiwavelength, UV to I, coverage of the images offers the baseline necessary to determine accurate ages of the stellar populations from colors.

The paper is organized as follows. The data are presented in Section 2 and the observed morphology of the ionized gas and of the stellar continuum is presented in Section 3. Section 4 investigates the effects of dust reddening on the photometric quantities; the results from this section are used in Section 5 to break the age/reddening degeneracy and derive the ages of the stellar populations and the recent star formation history of the galaxy. The summary is given in Section 6.

2. The Observations and the Data Reduction

NGC5253 was observed on May 8-9, 1996 with the HST WFPC2, in the broad band filters F547M and F814W and in the narrow band filters F487N and F656N. The log of the exposures, together with the exposure times and the characteristics of the filters are listed in Table 1. The starforming core of the galaxy is about 20''-30'' in diameter and was centered on the WF3 chip $(80'' \times 80'')$. A telescope orientation of about 85 degrees was requested to match the position and

orientation of archival WFPC2 images of the same region in the F255W filter (GO program # 6124, P.I. Robert Fesen); a homogeneous set of data covering the UV and optical wavelength range was therefore obtained. The final positional displacement of our images relative to the archival images is only a few pixels, and the relative rotation is 0.25 degrees.

Two pairs of images were obtained in each of the optical filters, with the second pair shifted by (5,5) pixels relative to the first pair (cf. Table 1). The F814W filter is the WFPC2 I band; the F547M filter is used here as a V band equivalent, and was preferred to the wider F555W filter because its bandpass excludes the strong [OIII](5007 Å) nebular emission from the galaxy. The recession velocity of NGC5253 is sufficiently small (404 km s⁻¹) that the two narrow band filters are almost centered at the wavelength of the hydrogen recombination emission lines H β (4861 Å) and H α (6563 Å), respectively. The F656N filter is narrow enough to exclude the redshifted [NII](6584 Å) emission line, while the [NII](6548 Å) emission line represents less than 2-3% of the H α flux in this low metallicity galaxy, as inferred from spectroscopic data (Storchi-Bergmann, Calzetti, & Kinney 1994). The archival dataset includes nine images obtained in the ultraviolet F255W filter on May 29, 1995. The images are organized in three triplets, with the second and the third triplet shifted by (-5,5) and (5,5) pixels relative to the first (see Table 1).

The data, both new and archival, were reduced by the STScI calibration pipeline, which includes flagging of bad pixels, A/D conversion, bias and dark current subtraction, flatfielding. We repeated the flatfield procedure on the optical images using the new flatfields available as of July 1996. The differences in the WF3 between old and new flatfields is of the order of 2% or less (peak-to-peak). The reduced images were registered to a common position using linear shifts; cosmic ray and hot pixel rejection and co-addition were performed using the STSDAS routine CRREJ (Williams et al. 1996), with a rejection threshold of 4 σ for the cosmic rays and 2.4 σ for the adjacent pixels.

The absolute photometric calibration of the images is obtained from the zero-points listed in HST Data Handbook (1995). The effect of contaminant buildup onto the WFPC2 window is negligible at optical wavelengths, but is important in the UV filters. The F255W observations were obtained 22.8 days after decontamination, with a net loss in efficiency of about 11%. The UV images have, therefore, been corrected for this effect.

The accuracy of the photometric calibration of the stellar continuum was checked against the UV (IUE) and optical spectrum of Kinney et al. (1993) and Storchi-Bergmann et al. (1995). To compare the WFPC2 images with the spectrum, fluxes were extracted from the images using the same aperture size and orientation of the spectrum. The aperture was centered at the peak of the optical emission in the images (about the center of the WF3 chip). The flux densities as measured from the images are only a few percent away from the values obtained from the spectrum convolved with the WFPC2 filters bandpasses (Table 2). The photometric zero-point has an accuracy of the order of 2-3% in the optical filters (HST Data Handbook 1995). The main source of uncertainty for the optical image-spectrum comparison is the background subtraction; the galaxy

has dimensions 5.00×1.95 (calculated at the blue surface brightness level of 25 mag arcsec⁻², de Vaucouleurs et al. 1991) and the galaxy's emission fills both the WF3 chip and the spectroscopic slit. This carries an uncertainty of the order of 5–6% in the background subtraction for both the V and I bands (see Table 2). A correction of 2% on the total counts is applied to the UV and the narrow-band images to correct for the Charge Transfer Efficiency (CTE) problem of WFPC2 (Holtzmann et al. 1995). The photometric zero-point for the F255W is known to within 5–7%, and an additional 3–4% uncertainty comes from the pointing uncertaity of the IUE.

Images of the nebular emission in $H\alpha$ and in $H\beta$ are obtained by subtracting the stellar continuum from the narrow band images. The image of the stellar continuum underlying the $H\alpha$ emission has been obtained by linear interpolation of the F547M and the F814W images to the central wavelength of the F656N image. The interpolated image has been multiplied by 1.10 to correct for a small disagreement in the stellar fluxes between the F656N and the interpolated images. Because of the galaxy's recession velocity, the $H\alpha$ emission line is 8.1 Å off-center in the filter bandpass and a small correction for the filter transmission (+9.4%) is applied.

For the stellar continuum underlying the H β emission, a linear extrapolation from the F547M and F814W images is adopted. This procedure potentially leads to larger uncertainties than for H α , because of differences in the blue continuum in blue and red stars. An 8% increase is applied to the extrapolated continuum images to match the intensity of stars to the level of the F487N images. A correction for the filter transmission curve (+1.1%) is also applied. The effect of the underlying stellar absorption is larger for the weak H β emission than for H α . Using red stellar objects to scale the continuum image to the narrow-band image can introduce a bias in the continuum subtraction of the blue stars, depending on the red stellar population. For example, an F/G type population has a relatively high H β absorption equivalent width, which would lead to undersubtraction of the OB stars continuum; on the other hand, a K-type population with small Balmer equivalent widths (EWs) would lead to over-subtraction of the blue stellar continuum. In the following, we will evaluate this uncertainty on a case by case basis.

Comparison of emission line and stellar continuum fluxes shows good agreement between the WFPC2 images and the spectral data (see Table 2). The 500 second F656N images have two saturated pixels corresponding to the H α emission peak. The effect of the saturation is discussed in section 4.2.1; in the present context, the large apertures employed for the image-spectrum comparison limit the effect of the saturation on the measured H α flux to the 1.3% level.

3. The Morphology of the Ionized Gas and of the Stellar Continuum

At the distance of 4.1 Mpc (Sandage et al. 1994), the WF pixel size of 0. 1 corresponds to a spatial scale of 2 pc. Details over the typical scale of starforming regions, ~ 10 pc, can therefore be studied with our images.

Over scales of tens of arcseconds, the H α line emission is roughly circularly symmetric, with

many loops and filaments extending mostly radially off the central region (see Figure 1a, and cf. Graham 1981, Martin & Kennicutt 1995, Marlowe et al. 1995). Upon closer inspection, the high spatial resolution of the WFPC2 image reveals a wealth of complex structures in the ionized gas emission. The E-W dust lane which bisects the galaxy core along the minor axis is visible in the $H\alpha$ map (Figure 1b). North of the lane, around the high surface brightness region which identifies the nucleus, the morphology of the gas emission is dominated by filamentary emission and shell structures with scales of a few arcseconds. The peak of the H α emission is roughly located at the center of the nuclear region, and coincides with the position of a stellar cluster (NGC5253-5, see Table 3). About 1".3 NW of the H α peak, a multiple shell structure with radii of about 20 pc each is visible in Figure 1b. This is one of the positions where enhanced nitrogen enrichment has been measured by Kobulnicky et al. (1997). The other region of N enhancement found by the same authors is located about 1".7 S of the center of the multiple shell structure. East of the $H\alpha$ peak, a complex, roughly circular, structure of ionized gas of about 65 pc diameter is present. South of the dust lane, a number of HII regions is distributed in the core amid a low level diffuse gas emission. HII regions are a common feature across the entire $H\alpha$ image. Two shell nebulae of about 25 pc diameter are located about 125 pc ENE and about 280 pc SSE of the core, respectively. The first shell, and the brightest of the two, contains two blue stellar objects, possibly ionizing stars. At the edges of the frame, at a distance of about 0.7–0.8 kpc from the core, two extended filamentary structures can be discerned ESE and W of the galaxy's center.

The profile of the H α surface brightness is shown in Figure 2 in annuli of increasing distance from the peak. The slope of the H α surface brightness increases in absolute value from inside out, and three different regions can be identified in the plot. The inner region has a radius of about 3", has the flattest slope and has the highest surface brightness (the nucleus). The intermediate region has a radius of about 13" and includes the entire core of NGC5253. Outside the 13" radius, the intensity of the H α emission drops rapidly. The surface brightness of the H α emission remains bright relative to the underlying stellar continuum up to 20" from the center; the radially averaged EW(H α) is above 90 Å in the region. This implies that intense photo- and shock-ionization of the ionized gas, and the star formation, are active up to at least 400 pc from the core of the galaxy. The presence of individual expanding bubbles, and enhanced knots of emission, hundreds of parsecs from the core, support this picture.

The morphology of the stellar continuum is markedly different from the morphology of the ionized gas (see Figure 3; Martin & Kennicutt 1995). The E–W dust lane which bisects the core is seen in the stellar images as well, but the two regions North and South of the lane do not show the dichotomy of appearance shown by the H α image. Indeed, the core appears quite homogeneous in terms of overall structure and brightness. On small scales (a few arcseconds), the core shows an irregular morphology, which alternates spots of high and low stellar surface brightness, and is mostly due to the inhomogeneity of the dust distribution. The large scale (>15") elliptical isophotes of the stellar light profile are centered about 5".8 SSW of the cluster NGC5253-5. The position of the starburst nucleus is thus displaced relative to the center of the galaxy's stellar light

profile.

4. The Effects of Dust

The dust reddening affecting nebular and stellar continuum emission in the core of NGC5253 is analyzed in sections 4.1 and 4.2. In section 4.2, the specific cases of the stellar clusters and of the reddening in the dust lane are discussed separately from the diffuse stellar population (sections 4.2.1 and 4.2.2, respectively). The reader interested in a summary of the effects of dust in the galaxy can refer to section 4.3.

4.1. The Reddening of the Gas

The ${\rm H}\alpha/{\rm H}\beta$ emission line ratio provides a measure of the dust reddening affecting the ionized gas, since variations of the intrinsic ratio are less than 5% for a large range of electron temperature and density. The ${\rm H}\alpha$ and ${\rm H}\beta$ emission line images are thus used to construct a gas reddening map for NGC5253. The images are first smoothed through median filtering with a 3×3 pixel window to reduce noise fluctuations, and then ratioed while setting to zero all pixels which are within 1.5 σ of the noise level. The result is shown in Figure 4a. The WFPC2 images reveal in detail the complex structure of the dust geometry, where heavy obscuration alternates with almost reddening-free regions. The E-W dust lane is the most apparent dust formation, together with a filament which departs North of the lane and connects to the obscured starburst nucleus. The region of highest obscuration is in the starburst nucleus, with its peak about 0″.5 W of the ${\rm H}\alpha$ emission peak. Two other elongated regions of large reddening are located N-W and N-E of the nucleus.

The average value of the ${\rm H}\alpha/{\rm H}\beta$ ratio over the central region of NGC5253 is 3.35, corresponding to ${\rm A}_V{=}0.53$ for a foreground homogeneous dust distribution. The extinction from our Galaxy is ${\rm A}_V{=}0.16$ (Burstein & Heiles 1982), implying ${\rm A}_V{=}0.37$ for the average intrinsic reddening. Thus, NGC5253 appears almost reddening-free when the average over an extended region is considered, despite the complex morphology of the line ratio map. In the nucleus and in the dust lane the observed ${\rm H}\alpha/{\rm H}\beta$ ratio reaches values as large as ${\sim}6$ (values larger than 6 are dominated by the noise), corresponding to optical depths of at least ${\rm A}_V{\sim}2.2$ assuming only foreground dust; those regions are optically thick.

The $\mathrm{H}\alpha/\mathrm{H}\beta$ ratio map provides information on the spatial variations, integrated along the line of sight, of the reddening affecting the gas in the galaxy. However, heavily obscured areas are optically thick in both emission lines, and the $\mathrm{H}\alpha/\mathrm{H}\beta$ ratio does not constrain the total dust optical depth in these regions. In the following section, we combine line and continuum emission data to derive the reddening in mildly dusty regions ($\mathrm{A}_V \approx 1$ mag). For the opaque nucleus, radio observations from the literature are combined with our data to constrain the extinction.

4.2. The Reddening of the Stellar Continuum

The small scale spatial variations of the stellar surface brightness match very well the variations in reddening derived from the Balmer emission lines (cf. Figure 3b with 4a). In addition, the regions with the highest values of ${\rm H}\alpha/{\rm H}\beta$ correspond to the reddest regions in the 547–814 color map (Figures 4a and 4b). All this indicates a correlation between the dust obscuration of the stellar continuum and of the gas emission. To quantify this statement, the behavior of the colors 255–547 and 547–814 is analyzed as a function of $\log(H\alpha/H\beta)$ for the central $16''\times16''$ (Figures 5a and 5b). Each point corresponds to the average color in a $0''.5\times0''.5$ bin; the binning has been chosen to ensure that detections in each bandpass is at least 4 σ above the limit even in the most reddened, i.e., faintest, regions. The uncertainties due to photon statistics for a 6 σ detection, are $\delta(255-547)$ =0.11 and $\delta(547-814)$ =0.07. Most of our data are better than 6 σ detections. The typical uncertainty in the ${\rm H}\alpha/{\rm H}\beta$ ratio is of the order of 6%, due to imperfect knowledge of the correction for the underlying stellar absorption. Both the Spearman and Kendall nonparametric correlation tests show that the points in Figure 5a deviate 10.8 σ and in Figure 5b 11.9 σ , respectively, from the null correlation hypothesis. An increase in the reddening of the gas is therefore mirrored by a reddening of the mean stellar colors.

For a foreground, uniform dust distribution, the equation describing the color-versus-line ratio trend is a straight line defined as:

$$m_{\lambda_1} - m_{\lambda_2} = (m_{\lambda_1} - m_{\lambda_2})_0 + \frac{k_{\lambda_1} - k_{\lambda_2}}{0.4(k_{\beta} - k_{\alpha})} \log\left(\frac{R_{\alpha\beta}}{R_{0,\alpha\beta}}\right),$$
 (1)

where $(m_{\lambda_1} - m_{\lambda_2})_0$ is the intrinsic color of the stellar population, $R_{\alpha\beta}$ and $R_{0,\alpha\beta}$ are the observed and intrinsic $H\alpha/H\beta$ ratios, respectively, and $k_{\lambda}=A(\lambda)/E(B-V)$ is the total-to-selective extinction, calculated at the continuum wavelengths λ_1 and λ_2 and at the wavelengths of the nebular emission lines $H\beta$ and $H\alpha$. For the intrinsic $H\alpha/H\beta$ ratio in NGC5253 we adopt the value 2.84 (Kobulnicky et al. 1997). In general, the dust distribution will not be foreground and uniform, so we define an effective attenuation k'_{λ} and an effective reddening $k'_{\lambda_1} - k'_{\lambda_2}$ for Equation (1).

The best fit of Equation (1) to the points of Figures 5a and 5b (after correction for the foreground Galactic reddening E(B-V)=0.05, Burstein & Heiles 1982) yields the values:

$$(255 - 547)_0 = -1.33 \pm 0.15$$

$$(547 - 814)_0 = -0.66 \pm 0.05,$$
(2)

and

$$(k'_{255} - k'_{547})/(k'_{\beta} - k'_{\alpha}) = 1.20 \pm 0.14$$

$$(k'_{547} - k'_{814})/(k'_{\beta} - k'_{\alpha}) = 0.52 \pm 0.04.$$
(3)

The intrinsic colors $(255-547)_0$ and $(547-814)_0$ are not immediately comparable with the data at zero reddening in Figure 5 ($\log(H\alpha/H\beta) \simeq 0.45$); the large scatter in the data is due to the presence

of resolved stars and stellar clusters prevents the comparison. A cross-check for Equation (2) is obtained by measuring the colors of the lowest obscuration regions in the core, after removal of all identifiable clusters and stars. With this technique, the colors are $255-547=-1.1\pm0.1$ and $547-814=-0.66\pm0.06$, in remarkable agreement with the intrinsic colors obtained from the best fit (Equation (2)).

In order to understand the meaning of Equation (3), we should remember that, if the dust is located in a foreground homogeneous screen, the selective extinction $(A_V/E(B-V)\simeq 3.1, Cardelli, Clayton & Mathis 1989)$ gives:

$$\begin{aligned}
& \left[(k_{255} - k_{547})/(k_{\beta} - k_{\alpha}) \right]_{ISM} &= 3.07 \\
& \left[(k_{547} - k_{814})/(k_{\beta} - k_{\alpha}) \right]_{ISM} &= 1.13.
\end{aligned} \tag{4}$$

For diffuse ISM, this result is almost independent of the chosen extinction curve, since in the wavelength range 2600-9000 Å there is little difference among the mean interstellar extinctions of the Galaxy, the Large Magellanic Cloud, and the Small Magellanic Cloud (Seaton 1979, Fitzpatrick 1986, Bouchet et al. 1985). The comparison between Equation (3) and (4) shows that the ratio of the effective reddening of the stellar continuum to the effective reddening of the gas emission in NGC5253 is smaller, by more than a factor two, than the expected ratio in the case of foreground homogeneous dust. To understand whether this discrepancy is due to the stellar continuum or to the gas, it should be remembered that the difference $k'_{\beta} - k'_{\alpha}$ is maximum if the dust is foreground to the gas,

$$k'_{\beta} - k'_{\alpha} = k_{\beta} - k_{\alpha} = 1.16;$$

more complex geometries than the simple foreground screen or dust scattering into the line of sight will make the difference smaller (CKS94) and will exacerbate the discrepancy between Equation (3) and (4). In addition, the small value of the ratio $(k'_{547} - k'_{814})/(k'_{\beta} - k'_{\alpha})$ cannot be reproduced if the geometrical distribution of the dust is the same for gas and stars (CKS94, Calzetti, Kinney & Storchi-Bergmann 1996). $(k'_{547} - k'_{814})$ probes larger optical depths than $(k'_{\beta} - k'_{\alpha})$; however complex the dust distribution, if gas and stars "see" the same amount of dust, the ratio between the two quantities should be $(k'_{547} - k'_{814})/(k'_{\beta} - k'_{\alpha}) \ge 1.13$. Therefore, the discrepancy between Equations (3) and (4) implies that the dust affecting the stellar emission has a covering factor about one half that of the dust affecting the gas emission: the gas is associated with regions of higher dust content than the stars. One immediate consequence of this scenario is that emission lines and stellar continuum are subject to differential reddening, and the line EWs are no longer reddening-free quantities (CKS94, Calzetti 1997).

The results presented in this section should be intended as 'mean' reddening corrections for the stellar continuum in NGC5253. The large spread in the data points of Figure 5 does not allow us to consider such corrections as the 'true corrections' for each individual data point; rather, the corrections should be considered valid in a statistical sense.

4.2.1. Reddening of The Stellar Clusters

The reddening of the stellar clusters in the core of NGC5253 is analyzed on an individual basis, to aid the derivation of the clusters' ages in section 5.

Stellar clusters (see Table 3) generally populate areas of low dust reddening in the core of NGC5253, with the (possibly only) exception of NGC5253-5 (Figures 3b and 4a). The fact that clusters crowd in low dust extinction regions may be an observational bias, since heavily reddened clusters are more likely to go unnoticed. Alternatively, evolving stellar clusters may destroy or 'blow away' the surrounding dust, via massive star winds and supernova explosions. This will make the dust distribution inhomogeneous and create 'holes' in the galaxy's ISM, through which the clusters can be observed. Table 3 reports the astrometric and photometric properties of the six brightest stellar clusters in the core. The STMAG magnitude system will be used throughout the paper. Two of the clusters (NGC5253-4 and NGC5253-5) are in the starburst nucleus, North of the dust lane, while the other four are located South of the lane. The photometry of the clusters was carried out using a circular aperture of 0.5 radius, and subtracting the underlying stellar flux derived from a ring of 0.5 size. Increasing the inner radius of the sky annulus and/or the aperture size by a factor 2 introduces variations of $\delta(255-547) \simeq \pm 0.07$ and $\delta(547-814) \simeq \pm 0.06$ in the colors, and $\simeq 15-30\%$ in the fluxes. We adopt the variations in the colors as uncertainties; we do not attempt to correct absolute quantities for the aperture effects, but we bear in mind the presence of this effect. Since the clusters are all located within the central 130 pixels of the frame. geometrical distortion and CTE effects are negligible relative to the aperture effects (Holtzman et al. 1995). The clusters are all resolved in the WF images, with measured FWHMs in the range 0'.22-0'.37 (stars in the same field have typical FWHMs in the range 0'.13-0'.17). The deconvolved FWHMs correspond to physical sizes between 3.2 pc and 6.8 pc.

The emission line ratios indicate that corrections of the nebular emission for the underlying stellar absorption further reduce the already small reddening values of the clusters in Table 3. An underlying absorption of EW=2 Å at H α and H β (see McCall et al. 1985) has been assumed for all clusters. This correction has negligible impact on the large EW of the line emission of the clusters NGC5253-4 and NGC5253-5, for which a measurable residual reddening is present. To bracket a range of possibilities, the photometric quantities of the two clusters are corrected for dust obscuration assuming two dust scenarios: 1) the small stellar continuum reddening implied by Equation (3) applies, thus attributing to the clusters the same mean 'effective reddening' observed for the diffuse population; 2) the dust is entirely foreground to the cluster and Equation (4) applies. In the first case, the total-to-selective obscuration value derived by Calzetti (1997) is adopted. A foreground dust distribution ($k'_{\beta} - k'_{\alpha} = 1.16$) is assumed for the reddening of the gas. The difference in the final photometry given by the different scenarios provide a measure of the uncertainties introduced by the dust effects.

The very blue cluster NGC5253-4 'sits' at the edge of the obscured nucleus (see Figures 3b and 4a). Despite its location, the emission from NGC5253-4 suffers relatively low dust reddening;

the cluster is either situated on the foreground surface of the otherwise obscured nucleus, or its massive star winds have succeeded in removing the blanket of dust in front of the cluster during the past few Myr. We favor the stellar winds mechanism, because the entire region surrounding the cluster is characterized by low obscuration. Uncertainties in the reddening corrections have small effect on the age determination of this cluster.

NGC5253-5 is the youngest cluster in the galaxy, with an age around 2.5 Myr (see section 5.2.1). The cluster is located roughly at the center of the starburst nucleus, in a region characterized by some of the largest values of the ratio $H\alpha/H\beta$. The central two pixels of the $H\alpha$ emission from the cluster are saturated; the correction to the saturation has been determined assuming that the $H\alpha/H\beta$ ratio of the saturated pixels is the same as the ratio of the neighbouring unsaturated pixels. The correction for the $H\alpha$ flux is 26% in the 0".5 aperture, if the dust is foreground; this is a lower limit, since more complex distributions of dust will yield larger corrections for the $H\alpha$. The observed colors (Table 3) are much redder than the values 255-547=-2.5 and 547-814=-1.1 expected for a 2-3 Myr old cluster, and the correction for reddening according to the two scenarios above is not sufficient to account for the discrepancy. Possibly the two models give inadequate reddening corrections for this cluster. The alternative possibility, that NGC5253-5 harbors an AGN, has been excluded by analyses of the high excitation lines (e.g., Lutz et al. 1996); in addition, the observed colors of this source are too blue for it to be an AGN (cf. Francis et al. 1991).

Hence, the first hypothesis is likely to be true: the adopted models for the reddening are inadequate. Indeed, such a young cluster would be still embedded in the molecular cloud from which it originated. The light from stars mixed with dust is subject to almost gray extinction at large optical depths τ , since the flux reduction due to obscuration becomes proportional to $1/\tau$: the spectral energy distribution of the emitting object will appear almost unreddened even in the presence of large amounts of dust (Natta & Panagia 1984, CKS94). A homogeneously mixed distribution of dust, stars and gas is thus an efficient way to 'hide' dust. In particular, the Balmer ratio is no longer a good diagnostic of extinction: the maximum value for the reddening between H α and H β , $A_{\beta\alpha} = A_{\beta} - A_{\alpha}$, is 0.25 mag, for a dust cloud with $A_V > 9$ mag. We measure $A_{\beta\alpha}=0.35$ mag in front of NGC5253-5, implying that a small amount of dust (A_V ~0.3 mag) must be foreground to the cluster to account for the additional $A_{\beta\alpha}=(0.35-0.25)=0.1$ mag. The following dust geometry in and around NGC5253-5 can account for the observed colors: the cluster is behind a relatively thin dust layer with $A_V \sim 0.3$ mag, and is completely embedded in a thick dust cloud with $A_V > 9$ mag. The colors and fluxes obtained from this dust model are shown in Table 3, where we consider also the case that the thin dust layer has optical depth $A_V=0.45$, the maximum value allowed by the uncertainties. Even after the new correction for reddening, the 547-814 color remains quite red relative to expectations for clusters of a few Myr age, while the 255-547 color is in close agreement with expectations; we cannot exclude a contribution from red stars foreground to the cluster.

Radio observations can help constraint the total obscuration in the direction of NGC5253-5,

since dust has little or no effect on radio emission. The position of the cluster is 1".3 East and 0".7 South of the 2 cm emission peak detected by Beck et al. (1996). The 2 cm emission from the nucleus of the galaxy has been shown to be 95% due to free-free emission from the ionized gas, so the ratio between the H β flux of NGC5253-5 and the radio emission can be used to derive the total extinction towards the cluster. The ratio of the emissivities between $H\beta$ and the radio is $j_{\beta}/j_{2cm}=3.738\times10^{-10}~{\rm erg~s^{-1}cm^{-2}Jy^{-1}}$ (Caplan & Deharveng 1986) for a nebula with electron temperature $T_e=10^4$ K. The flux at 2 cm is 23 mJy in the central radio source (Beck et al. 1996), implying a flux of 8.6×10^{-12} erg s⁻¹cm⁻² for H β . The observed H β flux (after correction for Galactic extinction) is 1.40×10^{-13} erg s⁻¹cm⁻². To recover the large flux implied by the radio emission, the stellar cluster should be embedded in a dust cloud with a total optical depth of 35 mag, for a homogeneous mixture of dust and stars. Again, a purely foreground dust distribution is ruled out by the observed colors of the cluster. We have implicitly assumed that the position of the optical peak is coincident with the radio peak, and that the observed difference of 1".5 is due to astrometric uncertainties. We cannot entirely exclude that the displacement between the two peaks is real and the radio peak emerges from a region of higher dust obscuration than the optical peak. Also the FWHM of the radio peak, about 0".8 (Beck et al. 1996), is larger than the FWHM=0".35 of the ionized gas peak. The conclusion is that NGC5253-5 is embedded in a dust cloud of optical depth between 9 and 35 mag at V (cf. Aitken et al. 1982).

4.2.2. The Dust Lane

The E-W dust lane suggests a dust geometry that is relatively easy to model – a sheet of dust (albeit inhomogeneous) embedded in a distribution of stars. To test this geometry, we extract photometry on either side of the lane and within it. We assume that the diffuse stellar population doesn't drastically change as a function of location in and around the lane, except for a decreasing intrinsic surface brightness as a function of the distance from the galaxy center. Additional constraints are added by the $EW(H\alpha)$; areas as close as possible in $EW(H\alpha)$ are selected within and outside the dust lane, to minimize differences in the stellar population. Eight areas, three within the dust lane, and five adjacent the lane, are identified, with 140 Å<EW(H α) <210 Å. Each of the eight regions is a square of 15 pixels on the side; the size is selected large enough to be roughly insensitive to local variations in the diffuse stellar population; for the same reason, the regions outside the dust lane are chosen as close as possible to the lane itself, mantaining that they must be external to the area of high reddening. The colors of these regions become redder for increasing values of the observed $H\alpha/H\beta$ (Figure 6). We interpret this result as an effect of dust reddening, rather than a change in the intrinsic stellar population, for the following reason. If the eight areas are radiation bounded, the observed values of $EW(H\alpha)$ imply an age range 150–500 Myr and a variation in intrinsic colors $\delta(255-547)<0.33$ and $\delta(547-814)<0.03$ for continuous star formation (Leitherer & Heckman 1995, LH95 hereafter). The observed range of colors in Figure 6 is larger than what expected from age variations in the stellar population.

Equation(1) is shown in Figure 6 overlaid on top of the data, using both Equations (3) and (4) for the selective reddening. Equation (3) is in better agreement with the data than the simple foreground dust geometry, implying, again, that the stellar continuum is on average less reddened than the gas emission. The dereddened colors for these regions are $(255-547)_0 \simeq -1.4$ and $(547-814)_0 \simeq -0.7$, corresponding to stellar population undergoing constant star formation over the past 200 Myr (Bruzual & Charlot 1995, BC95 hereafter), in agreement with the age range derived from the reddening-corrected values of EW(H α). This check ensures that Equation (3) gives a reasonable correction for the effects of dust extinction in the region.

For our geometrical model, we assume the dust lane corresponds to a clumpy layer of dust; regions of higher reddening correspond to a larger number of clumps along the line of sight. We allow a fraction f_s of stars to be foreground to the lane, therefore 'sandwiching' it. The fraction f_q of foreground gas is implicitly set to zero in this model, because the quantity $\log(H\alpha/H\beta)$ is assumed to scale linearly with the reddening. The dust clumps are assumed to be all equal and Poissonian distributed (Natta & Panagia 1984, see also CKS94). The optical depth of the clumps at different wavelengths is described by the SMC extinction curve (Gordon, Calzetti & Witt 1997); we also allow for the presence of scattered light into the line of sight. Free parameters in this 'sandwich' dust model are: the optical depth of each clump and the fraction f_s of foreground stars. The intrinsic colors of the stellar population are assumed to be in the range $-1.6 < (255-547)_0 < -1.0$ and $-0.80 < (547-814)_0 < -0.60$. The best fit model (shown in Figure 6) is given for $A_V(\text{clump}) = 0.16 \pm 0.02$, $f_s = 0.10 \pm 0.01$, and zero scattered light into the line of sight from external regions. The dust lane corresponds to an optical depth $A_V(\text{lane}) \simeq 2.2$. 10% of the stars are in front of both the dust and the gas; therefore the stars contributing to the UV and optical continuum emission must have a scale length larger than the ionized gas and must 'sandwich' the dust lane to account for their reddening properties.

4.3. Discussion: Dust in NGC5253

Corrections for the effects of dust extinction are crucial even in the case of a metal-poor dwarf galaxy like NGC5253. The inhomogeneity of the dust distribution is the key to interpret the many observational facts about the galaxy. Despite the obvious presence of dust, large aperture spectroscopy usually measures small reddening values (CKS94). This behavior can be attributed partly to the mixed dust/star/gas geometry of the nucleus, which produces almost gray extinction, and partly to the intrinsically low reddening observed in most of the galaxy's core.

Overall, the diffuse stellar population in the core is affected by a smaller reddening than the ionized gas. This discrepancy in obscuration between gas and stars is a common property of starburst galaxies (CKS94, Fanelli, O'Connell & Thuan 1988). The observed properties are accounted for if the dust has a larger covering factor in front of the ionized gas than in front of the stars. In the same vein, the scale length of stars may be larger than the scale length of the dust and of the gas emission. The stars located in low reddening regions do not contribute

significantly to the ionization of the gas, and/or are not associated with ionized gas, although they still contribute to the UV emission. In the first scenario, holes in the ISM may have been created by the massive star winds and supernova explosions of ageing stellar populations, and presently older stars "shine" through these holes. In the second scenario, nonionizing stars, which have longer lifetimes than ionizing stars, diffuse across the galaxy. Stars have typical dispersion velocities of 10 km s⁻¹ in our Galaxy, and the brightest O stars have a lifetime of approximately 3 Myr: they would travel only 30 pc from their place of birth over their life, while less massive stars would travel longer distances. In NGC5253, the half-light radius of the H β emission in the WF3 is $R_e=6''$, while it is $R_e=12''.5$ for the UV stellar emission. The ionized gas emission in this galaxy is thus more concentrated than the blue stellar light, and emerges from the heavily obscured starburst nucleus, while the UV-emitting stars are distributed across the galaxy's starforming core. The two scenarios, holes in the ISM and stellar diffusion, are not mutually exclusive, and both can account for the observed behavior of the stellar reddening. CKS94 derived an effective obscuration curve for the stellar continuum in starbursts (see, also, Calzetti 1997, Gordon et al. 1997) which folds together dust extinction and geometrical effects; this curve reproduces well the values of the selective reddening reported in Equation (3) and can therefore be used to describe the reddening characteristics of the stellar continuum in NGC5253.

Young starburst regions tend to be obscured: here the massive star winds and the supernova explosions have not had time to blow away the dust of the parental cloud in which the stars are embedded. In the nucleus of NGC5253, the almost complete absence of non-thermal radio emission (e.g., Beck et al. 1996) confirms that there have not been yet enough supernova explosions to help this process. The dust geometry is therefore dominated by the presence of the molecular clouds. The reddening in the nucleus of NGC5253 is generally high, although largely variable, with optical depths at V which range from 0.4 mag to 10 mag, and possibly higher at the position of the cluster NGC5253-5, in agreement with results obtained from infrared data (e.g., Aitken 1982, Telesco et al. 1993). Models of foreground dust are not sufficient to account for the obscuration, and the dust needs to be mixed with the stars and the gas. Because of the proximity of the dust to the ionizing stars, the former can be efficiently heated to high temperatures, explaining the higher mid-infrared to far-infrared ratio of NGC5253 relative to other starburst galaxies (Roche et al. 1991, Telesco et al. 1993, see, also, Calzetti et al. 1995). A complete description of the complex geometry of the nucleus is not possible with the data in hand, due to the limited range of optical depth sampled by the UV and optical data. Such a study would be immensely helped by high spatial resolution infrared mapping, as possible with the NICMOS instrument onboard HST.

5. The Ages of the Stellar Populations

The results from section 4 are used here to break the age/reddening degeneracy and derive ages for the diffuse stellar population (section 5.1) and for the stellar clusters (section 5.2). The age information is used in section 5.3 to derive a picture of the recent star formation history in the

core of NGC5253.

5.1. The Diffuse Stellar Population

Constraints on the age of the diffuse stellar population can be derived from color-color diagrams and from the EW of the emission lines. Figure 7 shows the colors of the galaxy's mean stellar population integrated along the line of sight for the central 16"×16", corresponding to a physical region of 320×320 pc². The mean value of the colors is not dominated by the contribution from resolved stars, as it does not depend on the size of the bins selected to calculate the colors themselves; however, the spread in the data is probably dominated by such effect (see the discussion in section 4.2). The contribution of the sky emission to the 547 and 814 bands is about 5% and 6%, respectively, and is negligible in the 255 band. To correct the colors for the effects of dust reddening, Equations (1) and (3) are applied to the data points. The $EW(H\alpha)$ is corrected for differential reddening between gas emission and stellar continuum using the results from section 4.2 and the total-to-selective reddening of Calzetti (1997): the difference in effective reddening between gas and stars is $k_{H\alpha}^g - k_{H\alpha}^s \simeq 0.48$. The reddening-corrected colors and EW are reported in Figures 8a-c. The comparison between Figure 7 and 8a shows the importance of reddening correction even in the case of a metal-poor galaxy like NGC5253: the 255-547 color becomes bluer by about -0.5 mag in mean value after the effects of dust are removed, leading to a factor 2 smaller inferred age for the stellar population.

Synthetic models of stellar populations must be employed to connect colors and EWs to ages. The population synthesis models of BC95 are plotted in Figure 8a for different age values of a stellar population undergoing constant star formation with a Salpeter (α =2.35) IMF in the stellar mass range $0.1-100 \text{ M}_{\odot}$. Although NGC5253 has metallicity 1/5-1/6 solar (e.g., Walsh & Roy 1989), the solar abundance BC95 models are adopted here; models with sub-solar abundances are still inadequate to account for the colors of red supergiants, and therefore the optical-IR colors of evolving populations (Goldader, Leitherer & Schaerer 1997). The contribution of the nebular continuum, taken from LH95, has been added to the BC95 stellar population spectra, before producing synthetic colors in STMAG via the STSDAS task SYNPHOT. Uncertainties on the photometric zero-point are included in the error-bar shown in Figure 8a. The variations of $EW(H\alpha)$ for constant star formation as a function of age are from LH95 (Figures 8b-c). The data cover the age range between 5×10^7 yr and 1 Gyr, with the peak of the distribution in the interval 100–500 Myr. This age range should be considered an effective age, meaning that different combinations of stellar populations can produce the same colors and $EW(H\alpha)$. The colors of the regions with the highest values of $EW(H\alpha)$ appear undercorrected for reddening (see Figures 8b-c). Such high values of the EW are likely to be associated with very young stellar populations; for these regions, the dust obscuration may be more complex than described by Equations (1) and (3)); furthermore, the continuous star formation assumption may be inadequate. Finally, $EW(H\alpha)$ may not be a good age discriminant if the gas is ionized by stars other than the underlying ones,

or if the emission is non-thermal.

There are reasons to believe that the nucleus contains a stellar population which is younger than the population in the core as a whole; the detection of W-R stars and the mean $EW(H\alpha)\sim 1000$ Å indicate the presence of a starforming population with an age of a few Myr in the nucleus. This young stellar population is not entirely identifiable with the two nuclear stellar clusters, NGC5253-4 and NGC5253-5, since the total H α flux and the total number of W-R stars are larger than what can be accounted for by the two clusters (see section 5.2.1). Unlike the case of the core population, the reddening-corrected color-color diagram of the nuclear region is not in agreement with either models of constant star formation or of instantaneous burst populations (Figure 9). The color 547–814 is the most deviant from the models; this apparent "undercorrection" of the red bandpasses relative to the blue bandpasses is typical of when foreground reddening corrections are applied to regions where the dust is actually mixed with the stars (cf. Natta & Panagia 1984, CKS94). From the 255-547 colors of the starburst nucleus, the age limits are <100 Myr for continuous star formation, and <20 Myr for an instantaneous burst population. More stringent age limits can be placed from the EW of the nebular lines: 95% of the data points have EW(H α)>250 Å and EW(H β)>65 Å, implying ages <20 Myr for constant star formation and <5 Myr for an instantaneous burst. The peaks of the distributions are at $EW(H\alpha)=1400 \text{ Å}$ and $EW(H\beta)=280 \text{ Å}$ consistent with ages of $\sim 5 \text{ Myr}$ and 3 Myr for constant star formation and instantaneous burst, respectively (LH95). As already mentioned, the ionized gas is probably not co-spatial with the ionizing stars; we expect that the EW of the Balmer emission lines place an upper limit to the age of the starburst nucleus.

5.2. The Stellar Clusters

We assume that each stellar cluster can be described by a co-eval stellar population and use instantaneous burst population models to estimate its age from the colors and the EW of the H α and H β lines. The latter are treated only as upper limits to the ages, since our aperture (equivalent to about 10 pc) may not include all of the emission line gas ionized by the stellar cluster.

Models of instantaneous burst populations are constructed from both empirical stellar libraries (BC95) and theoretical stellar libraries (LH95 and Bruzual & Charlot 1996, BC96 hereafter) using solar metallicity and Salpeter IMF in the range 0.1–100 M_{\odot} . Contribution of the nebular continuum to the colors from LH95 is added to all the models. The two types of libraries differ in the predicted colors. The 547−814 color predicted by BC95 is systematically redder by 0.2–0.3 mag than that predicted by LH95 and BC96 for ages >7−8 Myr. The four clusters older than 8 Myr in our sample (see Table 3) have 547−814 in better agreement with BC95 than with the other models. BC95 predicts 255−547 colors which are about 0.3 mag redder than LH95 and BC96. This effect is attributed to inadequate correction for reddening of the massive stars in the spectral library of BC95, which produces a 30% depression of the UV flux at 2600 Å in the stellar population models. The uncertainties from the models, together with the uncertainties

from the reddening corrections, are factored in the final age value of each cluster. Age estimates on the basis of the EW of H α and H β are done using the LH95 models. The derived age ranges are listed in the last column of Table 3.

5.2.1. Clusters in the Starburst Nucleus.

The cluster NGC5253-5, which resides in the center of the starburst nucleus, is the youngest cluster in the galaxy: the EW of its $H\beta$ emission indicates an age of 2.2 Myr, while the EW of $H\alpha$ indicates an upper limit to the age around 2.8 Myr. The FWHM of the H α emission at the position of the cluster is comparable with the FWHM of the stellar emission from the cluster, suggesting that the ionized gas is as concentrated as the stellar cluster and, likely, co-spatial. The total $H\alpha$ emission within an aperture of 0'.5 radius centered on NGC5253-5 is 5.84×10^{-13} erg s⁻¹cm⁻², with an uncertainty around 10%, due mostly to uncertainty in the saturation correction. Of this flux, about 80% comes from the cluster proper (cf. Table 3); the remaining 20% can be attributed to photoionization from the diffusely distributed stars in the nuclear region (as inferred from the H α intensity surrounding the cluster). As seen in section 4.2.1, the colors of NGC5253-5 cannot be used as effectively as the EW of the emission lines to derive an age because of the heavy reddening in the direction of this cluster. The detection of a Wolf-Rayet feature in the spectrum of NGC5253-5 (Schaerer et al. 1997) indicates an age of at least 3 Myr, a slightly greater value than derived from the nebular lines. The feature detected by Schaerer and collaborators may be due to very massive (M $\sim 100 \text{ M}_{\odot}$) stars with strong mass loss which mimic Wolf-Rayet stars; these stars are 2 Myr old at most, and are thus still on the main sequence (de Koter, Heap, & Hubery 1997). In addition, the cluster is located on top of a generally active starforming area a few arcseconds in size which may include W-R stars, a fraction of which would be encompassed by the slit aperture used by Schaerer et al.

If the dust cloud in which NGC5253-5 is embedded has optical depth A_V =35 mag, the intrinsic optical magnitude of the cluster is m_{547} =13.5, corresponding to M_V =-14.5, and a mass in stars of about 10^6 M_{\odot} , for the adopted IMF. On the basis of its absolute magnitude and its half-light radius, $R_e \sim 3.5$ pc, NGC5253-5 can be classified as a 'super-star-cluster', comparing well to the super-star-clusters in other blue compact dwarf galaxies NGC1705 (Meurer et al. 1992), NGC1569 (O'Connell, Gallagher & Hunter 1994), He2-10 (Conti & Vacca 1994), as well as in other starburst galaxies (Hunter, O'Connell & Gallagher 1994, Watson et al. 1996). Even assuming that there are "only" 9 mag of optical extinction towards NGC5253-5, the rate of ionizing photons, 1×10^{52} photons/s, and the intrinsic optical magnitude, M_V =-13, correspond to a mass in stars of about 2-3×10⁵ M_{\odot} : NGC5253-5 thus remains a massive cluster.

NGC5253-4 is the brightest and has the bluest observed colors among the UV stellar clusters in the core of NGC5253 (Meurer et al. 1995). A young age and the low dust reddening are implied by the observed characteristics. The total H α flux within the 0".5 radius aperture is 1.70×10^{-13} , comparable to the flux measured by Kobulnicky et al. (1997) from their FOS spectrum in the 0".9

diameter aperture; the background-subtracted H α flux is only 70% of that value (Table 3). As in the case of NGC5253-5 the remaining 30% of the H α flux can be attributed to the underlying starburst population. The colors indicate an age around 2.5 Myr, while the EW of the hydrogen recombination lines indicate an upper limit to the age between 4.0 and 4.4 Myr. The properties of NGC5253-4 are well explained by a moderately aged instantaneous burst of star formation. Our derived age is confirmed by the detection of Wolf-Rayet stars in this cluster, which constrains the age to be around 3-4 Myr (Schaerer et al. 1997). The number of ionizing photons currently produced by the cluster is $\sim 2.5 \times 10^{50}$ photons/s, corresponding to a total number of about 25 O stars (LH95). The typical WR/O ratio is between 1/3 and 1/10, implying that at most 5-8 WR stars should be present in NGC5253-4 (Vacca & Conti 1992, LH95). Of the 42 WR stars detected by Schaerer et al. in their 1".6 long slit aperture spectrum, only about 1/5 are thus associated with the stellar cluster, while the others are probably associated with the diffuse starburst population. Indeed, NGC5253-4 is surrounded by a number of resolved blue stars which appear to be associated with the cluster, though they may not be gravitationally bound to it. The total mass in stars of NGC5253-4 is about 1.3×10^4 M_{\odot}. A similar number for the mass in stars, 4×10^4 M_{\odot}, is obtained from the F547M magnitude (LH95). NGC5253-4 is therefore a relatively small cluster, even for an IMF which extends down to 0.1 M_{\odot} . Its absolute magnitude, $M_V \simeq M_{547} = -11$, is comparable to the absolute magnitude of R136 in 30 Doradus (e.g., Leitherer 1997), and the cluster has half-light radius $R_e=3$ pc, slightly smaller than the radius of NGC5253-5.

The youth of NGC5253-4 and NGC5253-5 is consistent with the age range derived for the diffuse stellar population in the nucleus (see previous section) and the almost complete absence of non-thermal radio emission in the center of NGC5253 (e.g., Beck et al. 1996): the first supernovae are expected to explode after 3–4 Myr (LH95), and the region has not yet or has just reached that stage.

The ratio of the 2 cm emission from the compact source to the 2 cm emission from the entire nucleus is about 2/3 (Beck et al. 1996). If the ratio of ionizing photons from the clusters and from the nucleus is approximately the same, 65% of the nuclear star formation is happening in the two clusters. At minimum, 20% of the nuclear star formation is happening in the two clusters, as inferred from the ratio of the H α flux from the clusters to the total H α emission from the region $(5.71\times10^{-12}~{\rm erg\,s^{-1}cm^{-2}})$, after correction for extinction). For comparison, the stellar clusters in the entire starforming core of NGC5253 represent at most 15% of the UV light. The contribution of cluster emission thus appears to be more important in the nucleus than in the core as a whole; the difference in age between nucleus and core suggests that cluster formation is an important mode of star formation in the early phases of a starburst event.

In order to derive ages for the stellar clusters and for the diffuse stellar population, the stellar IMF has been assumed a priori to be Salpeter-like (α =2.35) with mass range M=0.1–100 M $_{\odot}$. Some a posteriori considerations, based on the value of the EW(H β) of NGC5253-5, suggest that the assumption on the slope and the upper mass limit may be not too far from the reality. An upper mass limit of only 30 M $_{\odot}$ or a steeper IMF slope (α =3.3) would produce an EW of H β less

than half that observed. This is indirect evidence that the adopted values for the slope and the upper mass limit describe adequately the observed properties in NGC5253, in agreement with previous findings on dwarf galaxies (Massey et al. 1995, Stasińska & Leitherer 1996), and recent suggestions on massive galaxies (Calzetti 1997, Bresolin & Kennicutt 1997).

Note that some of the derived quantities, such as cluster masses and star formation intensities (see previous and next sections), are more sensitive to variations of the low-mass end of the IMF, for which we have no direct information. As an example, if the IMF low-mass cut-off is at 1 M_{\odot} rather than 0.1 M_{\odot} , all cluster masses and star formation intensities decrease by a factor 2.5.

5.2.2. Older Clusters in the Core

The other four of the stellar clusters of Table 3 are older than NGC5253-5 and NGC5253-4, with ages between 10 and 50 Myr, as determined from the colors. Their absolute magnitudes are in the range $M_V=-10$ to -11.3; because of aging, they have lost between 1 and 2.5 magnitudes relative to their peak brightness (LH95). Their masses are in the range $0.7-4\times10^5~M_{\odot}$. These clusters are comparable in mass to NGC5253-5, and are almost one order of magnitude more massive than NGC5253-4. Taken all together, the six clusters have half-light radii in the range $1.6-3.5~\rm pc$, and ages in the range $2-50~\rm Myr$. The oldest clusters tend to have the smallest radii: the two clusters in the nucleus have half-light radii in the range $3-3.5~\rm pc$, while the four other clusters have radii in the range $1.6-2.9~\rm pc$. The cluster's crossing time for a star with velocity $5~\rm km/s$ is less than 2 Myr; this implies that at least the four clusters older than 10 Myr are likely to be gravitationally bound, a suggestion supposerted by the decreasing radius for increasing age.

5.3. Discussion: Recent Star Formation

The bulk of the current star formation in NGC5253 is located in an area of radius $\sim 2.5^{\circ}-3^{\circ}$, i.e. 50–60 pc, in the North part of the core, centered at the position of the H α peak. The entire region appears not older than about 10 Myr, and is probably as young as 5 Myr. The age of the starburst is suggested by a series of clues: the region contains two very young clusters, with age between 2 and 4 Myr; the H α surface brightness is high, with an EW peaking above 1000 Å; the radio emission is almost entirely thermal (Beck et al. 1996); and the number of red supergiants is small (Campbell & Terlevich 1984). The two N-enriched regions in the starburst nucleus are probably observed when massive stars are polluting the medium (timescale of 10^6 yr), but before supernovae explosions can homogenize the ISM (timescale of 10^7 yr, Kobulnicky et al. 1997). The average star formation intensity in this area is between 10^{-5} and 10^{-4} M $_{\odot}$ /yr/pc 2 for a 0.1–100 M $_{\odot}$ Salpeter IMF, depending on the adopted value for the reddening. The value corresponds to the maximum starburst intensity found in galaxies (Meurer et al. 1997a).

In the part of the core South of the dust lane, the $H\alpha$ surface brightness is smoothly

distributed, except for a few isolated and relatively faint HII regions/complexes; the corresponding star formation rate is about $10^{-6} \text{ M}_{\odot}/\text{yr/pc}^2$, one to two orders of magnitude lower than in the nucleus. The ionized gas emission is probably produced by the same diffuse population(s), which is(are) responsible for the blue colors in the core of NGC5253. The four bright clusters with ages between 10 and 50 Myr are situated also south of the dust lane, within a region of about 10" in size, and have no longer a dominant role in ionizing the gas. These clusters appear to be the remnants of a past star formation episode in the region. A starburst event thus started about 50-100 Myr ago or earlier and produced clusters which have the same characteristics (luminosity, physical size) as the two young ones in the nucleus. Star formation is still going on in the core, albeit at a lower efficiency level than in the nucleus. The blue colors of the core are equivalent to a stellar population which is continuously forming stars since 100-500 Myr, in agreement with the above picture. The core of NGC5253 thus appears to have undergone two or more starburst episodes over the last ~ 100 Myr or so, or a continuous star formation episode of variable intensity. The oldest stellar clusters may, however, not be directly linked to the star formation history of the area where they are located. With a typical velocity dispersion of 46 km s⁻¹ (Caldwell & Phillips 1989), the crossing time of the core region (about 200 pc) is less than 10 Myr. The difference in age between the diffuse stellar populations in the nucleus and in the core as a whole explains the difference in the half-light radii between the UV stellar emission and the ionized gas emission ($R_e(UV)=12''.5$ versus $R_e(H\beta)=6''$) in NGC5253. While only stars more massive than $20\text{--}30~\mathrm{M}_{\odot}$ produce hard enough radiation to ionize the gas, stars with masses as low as 5–10 M_{\odot} can significantly contribute to the UV emission at 2600 Å. Typical lifetimes of the former are \sim 10 Myr, while the latter can live as long as 100 Myr or so.

The central starburst in NGC5253 is just the very last episode of a complex star formation history, of which we have glimpsed the last 100 Myr through the analysis of the stellar clusters and of the diffuse blue population. Burst durations have implications for the detection of the post-starburst galaxies. Norman (1991) calculated that if bursts of star formation are almost instantaneous events, as many starburst as post-starburst galaxies should be observed, after making allowances for the dimming of the aged burst. The number of observed post-starburst galaxies is much smaller than the number of starbursts, implying either that starbursts do not form A-type and lower mass stars or that bursts of star formation are long-lived events. Our results point in the direction of starbursts as long-lived events, although we cannot exclude that low mass stars do not form (cf. Calzetti 1997). A burst duration of 100 Myr reduces the post/burst ratio to about 1/2 (Norman 1991), and longer lifetimes reduce the ratio even further.

6. Summary

The analysis of the HST WFPC2 images of NGC5253 has shown that the observational peculiarities of this metal-poor dwarf galaxy are mostly driven by the combination of the dust distribution and of the evolution of the star formation in the core.

The dust is inhomogeneously distributed across the central $20'' \times 20''$, alternating regions of small and large reddening. On a scale of a few arcsec, areas of high obscuration for the gas are correlated with areas of high obscuration for the stellar continuum. The highest values of obscuration are found in the E-W dust lane and in the starburst nucleus. The former can be modeled by a clumpy dust layer of optical depth $A_V \simeq 2.2$, which is obscuring the gas and most of the stars located in the region; a small fraction, $\sim 10\%$, of the stars is in front of the dust lane, accounting for the smaller reddening of the stellar continuum relative to the ionized gas. In the nucleus, the configuration which explains the observed stellar colors is a homogeneous mix of dust, stars, and gas; the stars generated by the starburst are still embedded in the parental cloud, which has a total optical depth at V of 9–35 magnitudes (cf. Aitken 1982). The rest of the core region is compatible with relatively small values of the dust reddening, which however still imply corrections of about -0.5 mag in the 255-547 colors. This corresponds to a decrease in the age of the stellar populaiton of about a factor 2.

The simultaneous presence of an obscured starburst nucleus and an almost dust-free blue core accounts for both the intense UV and infrared emission. The starburst nucleus provides the bulk of the ionized gas emission: half of the $H\alpha$ flux from the galaxy is within a radius of 6'' from the peak of the emission. Mixed configurations of dust and gas produce almost grey extinction, accounting for the relatively small values of the reddening derived in the nucleus from the Balmer decrement. The UV light, on the other hand, comes from a larger region: half of the emission at 2600 Å is from a radius of 12". The bulk of the observed UV light is thus provided not by the young starburst nucleus, but by the core as a whole, which is older, almost unextincted, and is producing stars at an efficiency rate about 10 times lower than the nuclear starburst. The dichotomy in the origin of the ionized gas and UV stellar emission explains why the UV spectral energy distribution of the core is not as blue as expected for a young, unextincted starburst (Gonzalez-Riestra et al. 1987, CKS94). Despite the inhomogeneity of the dust distribution, a general result can be derived for the reddening correction in the center of NGC5253: the stellar continuum suffers on average about half the reddening of the gas emission. This behavior is typical of the nuclei of starburst galaxies, and is explained if the gas is more closely associated with the dust than the stars and much of the observed UV and optical continuum emission is provided by non ionizing stars located in low extinction area (CKS94, Calzetti 1997). The case study of NGC5253 has additionally demonstrated that the dichotomy in reddening behavior cannot be attributed to bulk diplacements between the stellar continuum and the ionized gas emission; in fact, the dichotomy holds, on average, down to scales of a few pc.

The six brightest stellar clusters in the core span an age range between 2 and 50 Myr. Age is the largest discriminant among them; other characteristics, such as absolute luminosities (scaled to a coeval value), sizes, and inferred masses, have similar values. Five of the clusters have masses around 10^5 M_{\odot} , for a Salpeter IMF extending down to 0.1 M $_{\odot}$. The half-light radii range from 1.6 to 3.5 pc, with the older clusters being more compact than the younger ones. The clusters are probably gravitationally bound. The two youngest clusters, with ages between 2 and 4 Myr,

produce between 20% and 65% of the ionizing photons in the nucleus, a higher fraction than produced by the clusters in the core, as expected if the early stage star formation is associated with cluster formation. The other four, older clusters (10-50 Myr) are located south of the starburst and are roughly co-eval with the diffuse starforming population of the core. There appears to be an anti-correlation between age and reddening of the cluster, with the youngest object being more heavily extincted than the oldest. Stellar clusters are thus borne completely enshrouded in the dust of the parental cloud, but after only 2–3 Myr, emerge from the cloud and become UV bright. The similarity among the six clusters in term of masses and sizes suggests that they were generated by similar processes.

The age range of the clusters and the intrinsic colors of the diffuse stellar population in the core suggest that star formation has been fairly active in the region, albeit with variable intensity, during at least the past 100 Myr. The current peak of star formation is more spatially concentrated than the star formation integrated over the last 100 Myr. The nuclear burst of star formation, with an average age around 5 Myr, thus represents only the last of a sequence of starburst episodes. The timescale of the star formation activity in the core may ultimately be much longer than 100–500 Myr; this analysis of the stellar population content of NGC5253 will be refined in a forthcoming paper (Meurer et al. 1997b).

The authors would like to thank Robert Fesen for providing information on the observing strategy adopted for the ultraviolet images of NGC5253. This research has made use of the NASA/IPAC Extragalactic Database (NED) which is operated by the Jet Propulsion Laboratory, California Institute of Technology, under contract with the National Aeronautics and Space Administration. During this work, G.R.M. and D.R.G. were supported by the NASA Grant GO-06524.01-95A.

REFERENCES

Aitken, D. K., Roche, P. F., Allen, M. C., & Pillips, M. M., 1982, MNRAS, 199, 31P

Babul, A., & Ferguson, H. C. 1996, ApJ, 458, 100

Beck, S. C., Turner, J. L., Ho, P. T., Lacy, J. H., & Kelly, D. M. 1996, ApJ, 457, 610

Bouchet, P., Lequeux, J., Maurice, E., Prevot, L, & Prevot-Burnichon, M. L. 1985, A&A, 149, 330

Bresolin, F., & Kennicutt, R. C. 1997, AJ, 113, 975

Bruzual, G. A., & Charlot, S. 1995, private communication

Bruzual, G. A., & Charlot, S. 1996, private communication

Burstein, D., & Heiles, C. 1982, AJ, 87, 1165

Caldwell, N., & Phillips, M. M. 1989, ApJ, 338, 789

Calzetti, D. 1997, AJ, 113, 162

Calzetti, D., Bohlin, R. C., Kinney, A. L., Storchi-Bergmann, T., & Heckman, T. M. 1995, ApJ, 443, 136

Calzetti, D., Kinney, A. L., & Storchi-Bergmann, T. 1994, ApJ, 429, 582

Calzetti, D., Kinney, A. L., & Storchi-Bergmann, T. 1996, ApJ, 458, 132

Campbell, A., & Terlevich, R., 1984, MNRAS, 211, 15

Campbell, A., Terlevich, R., & Melnick, J. 1986, MNRAS, 223, 811

Caplan, J., & Deharveng, L. 1986, A&A, 155, 297

Cardelli, J. A., Clayton, G. C., & Mathis, J. S. 1989, ApJ, 345, 245

Chu, Y. H., & Kennicutt, R. C. 1994, ApJ, 425, 720

Colless, M., Schade, D., Broadhurst, T., & Ellis, R., 1994, MNRAS, 267, 1108

Conti, P. S., & Vacca, W. D. 1994, ApJ, 423, L97

de Koter, A., Heap, S. R., & Hubeny, I. 1997, ApJ, 477, 792

de Vaucouleurs, G., de Vaucouleurs, A., Corwin, H. G., Buta, R. J., Paturel, G., & Fouqué, P. 1991, Third Reference Catalogue of Bright Galaxies (New York: Springer-Verlag)

Fanelli, M. N., O'Connell, R. W., & Thuan, T. X. 1988, ApJ, 334, 665

Fitzpatrick, E. L. 1986, AJ, 92, 1068

Francis, P. J, et al. 1991, ApJ, 373, 465

Gallego, J., Zamorano, J., Aragon-Salamanca, A., & Rego, M. 1995, ApJ, 455, L1

Giavalisco, M., Steidel, C.C., & Macchetto, F.M. 1996, ApJ, 470, 189

Goldader, J., Leitherer, C., & Schaerer, D. 1997, in preparation

Gonzalez-Riestra, R., Rego, M., & Zamorano, J. 1987, A&A, 186, 64

Gordon, K. D., Calzetti, D., & Witt, A. N. 1997, ApJ, accepted for publication

Graham, J. A. 1981, PASP, 93, 552

Heckman, T.M. 1997, in Star Formation Near and Far, the 7th Annual Astrphysics Conference in Maryland, S.S. Holt & L.G. Mundy eds. in press

Heckman, T.M., Armus, L., & Miley, G. 1990, ApJS, 74, 833

Holtzman, J., et al. 1995, PASP, 107, 156

Hunter, D. A., O'Connell, R. W., & Gallagher, J. S. 1994, AJ, 108, 84

Kinney, A. L., Bohlin, R. C., Calzetti, D., Panagia, N., & Wyse, R. F. G. 1993, ApJS, 86, 5

Kobulnicky, H. A., Skillman, E. D., 1995, ApJ, 454, L121

Kobulnicky, H. A., Skillman, E. D., Roy, J.-R., Walsh, J. R., & Rosa, M. R. 1996, ApJ, 477, 679

Lehnert, M. D., & Heckman, T. M. 1996, ApJ, 462, 651

Leitherer, C. 1997, in Starburst Activity in Galaxies, ed. J. Franco, R. Terlevich, & G. Tenorio-Tagle, Rev. Mex. Astron. Astrfis. Conf. Series, in press

Leitherer, C., & Heckman, T. M. 1995, ApJS96, 9

Lowenthal, J., Koo, D., Guzman, R., Gallego, J., Phillips, A., Faber, S., Vogt, N., Illingworth, G., & Gronwall C 1997, ApJ, in press

Lutz, D., Genzel, R., Sternberg., A., Netzer, H., Kunze, D., Rigopoulou, D., Sturm, E., Egami, E., Feuchtgruber, H., Moorwood, A. F. M., & de Graauw, Th. 1996, A&A, 315, L137

Marlowe, A. T., Heckman, T. M., Wyse, R. F. G., & Schommer, R. 1995, ApJ, 438, 563

Martin, C. L., & Kennicutt, R. C. 1995, ApJ, 447, 171

Massey, P., Lang, C.C., De Gioia-Eastwood, K., & Garmany, C.D. 1995, ApJ, 438, 188

McCall, M. L., Rybski, P. M., & Shields, G. A. 1985, ApJS, 57, 1

Meurer, G. R., Heckman, T. M., Leitherer, C., Kinney, A. L., Robert, C., & Garnett, D. R. 1995, AJ, 110, 2665

Meurer, G. R., Heckman, T. M., Lehnert, M. D., Leitherer, C., & Lowenthal, J. 1997, AJ, accepted for publication

Meurer, G. R., et al., 1997, in preparation

Meurer, G. R., Mackie, G., & Carignan, C. 1994, AJ, 107, 2021

Meurer, G. R., Freeman, K. C., Dopita, M. A., & Cacciari, C. 1992, AJ, 103, 60

Moffat, A. F. J. 1996, proceedings of the meeting "Starburst Activity in Galaxies", Puebla (Mexico), J. Franco, R. Terlevich, and G. Tenorio-Tagle eds.

Natta, A., & Panagia, N. 1984, ApJ, 287, 228

Norman, C. A. 1991, in Massive Stars in Starbursts, ed. C. Leitherer, N. R. Walborn, T. M. Heckman, & C. A. Norman, (Cambridge: Cambridge University Press), 271

O'Connell, R. W., Gallagher, J. S., & Hunter, D. A. 1994, ApJ, 433, 65

Olson, K., & Kwan, J. 1990, ApJ, 361, 426

Phillips, S., & Driver, S. 1995, MNRAS, 274, 832

Roche, P. F., Aitken, D. K., Smith, C. H., & Ward, M. J. 1991, MNRAS, 248, 606

Rogstad, D. H., Lockhart, I. A., & Wright, M. C. H. 1974, ApJ, 1 93, 309

Sandage, A., & Brucato, R. 1979, AJ, 84, 472

Sandage, A., Saha, A., Tamman, G. A., Labhardt, L., Schweneler, H., Panagia, N., & Macchetto, F. D. 1994, ApJ, 423, L13

Schaerer, D., Contini, T., Kunth, D., & Meynet, G. 1997, to appear in ApJ Letters.

Seaton, M. J. 1979, MNRAS, 187, 73P

Sérsic, J. L., Carranza, G., & Pastoriza, M. 1972, Ap&SS, 19, 469

Shlosman, I. 1992, in Relationships between Active Galactic Nuclei and Starburst Galaxies (San Francisco: ASP), A. V. Filippenko ed., 335

Shull, J. M. 1993, in Massive Stars: Their Lives in the Interstellar Medium, ed. J. P. Cassinelli & E. B. Churchwell (San Francisco: ASP), 327

Stasińska, G. & Leitherer, C. 1996, ApJS, 107, in press.

Steidel, C. C., Giavalisco, M., Pettini, M., Dickinson, M., & Adelberger, K. L. 1996, ApJ, 462, L17

Storchi-Bergmann, T., Calzetti, D., & Kinney, A. L. 1994, ApJ, 429, 572

Storchi-Bergmann, T., Kinney, A. L., & Challis, P. 1995, ApJS, 98, 103

Telesco, C. M., Dressel, L. L., & Wolstencroft, R. D. 1993, ApJ, 414, 120

Turner, J. L., Beck, S. C., & Hurt, R. L. 1997, ApJ, 474, L11

Vacca, W. D., & Conti, P. S. 1992, ApJ, 401, 543

van den Bergh, S. 1980, PASP, 92, 122

Walsh, J. R., & Roy, Roy, J.-R. 1987, ApJ, 319, L57

Walsh, J. R., & Roy, Roy, J.-R. 1989, MNRAS, 239, 297

Watson, A. M., et al. 1996, AJ, 112, 534

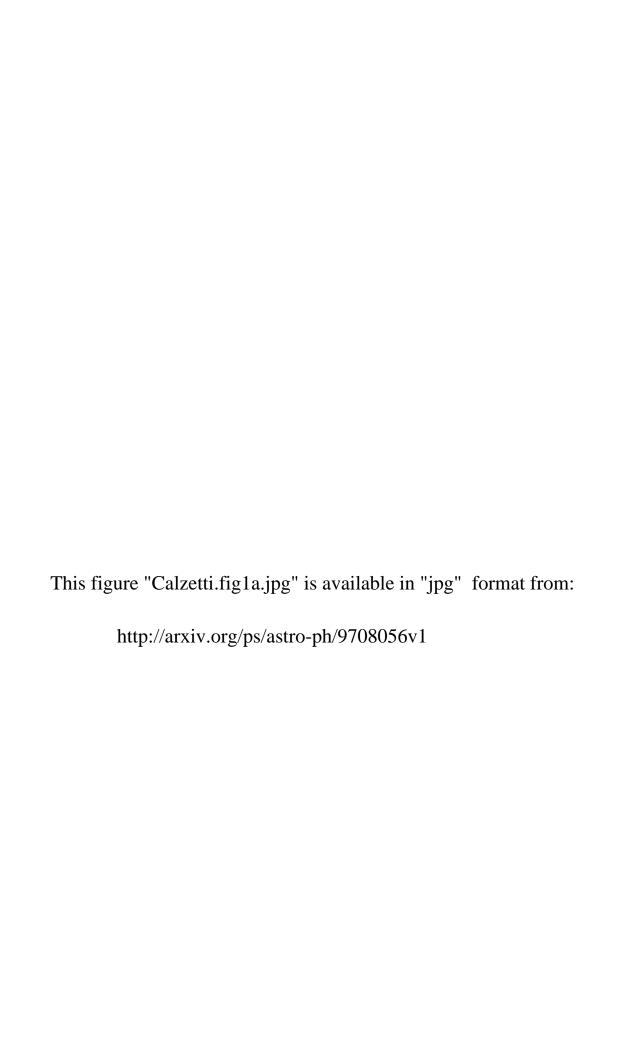
Williams, R. E. et al. 1996, AJ, 112, 1335

This preprint was prepared with the AAS IATEX macros v4.0.

- Fig. 1.— a) (Plate) The continuum-subtracted H α image; the scale is 52" on a side. North is up; East is left. The image is shown in logarithmic contrast to emphasyze the low surface brightness regions. b) (Plate) The inner 25"×25" detail of the H α emission; the contrast of the image is in linear scale.
- Fig. 2.— The continuum-subtracted H α surface brightness as a function of the distance from the central peak. The size of the 1 σ uncertainty is shown as an orizontal bar inside the circles of the data points.
- Fig. 3.— a) (Plate) Three-color image of the central $52'' \times 52''$ of NGC5253 in the stellar continuum at 2600 Å (F255W, blue), 5500 Å (F547M, green) and 8000 Å (F814W, red). North is up; East is left. The image has the same size, orientation, and position of the H α image of Figure 1a. b) (Plate) The F547M image of the inner $25'' \times 25''$. The scale and position are the same as Figure 1a. The six brightest stellar clusters are marked with the same ordering given in Table 3.
- Fig. 4.— a) (Plate) The $H\alpha/H\beta$ ratio image for the inner 25"×25". North is up; East is left. Light regions indicate small values of the line ratio (low reddening), while darker regions mark large values of the reddening. The white edges indicate lack of signal. Three spots 1–2 pixels wide of lighter shade can be discerned inside the central region; the spots correspond to the positions of stellar clusters, and the low value of $H\alpha/H\beta$ measured in those pixels is due to imperfect matching of the F487N and F656N PSFs and slight mis-registration. b) (Plate) The 547–814 map is shown on the same scale as the $H\alpha/H\beta$ image; regions of high reddening in the $H\alpha/H\beta$ map correspond to red colors (dark regions) in the stellar continuum map.
- Fig. 5.— a) The 255–547 color plotted as a function of the gas reddening indicator $H\alpha/H\beta$ for the inner 16"×16" of the galaxy. Each data point corresponds to a region 0".5 in size. The typical uncertainty on the data is reported at the top right of the plot. The vertical bar to the left of the data points represents the colors of the diffuse stellar population after removal of stellar clusters and resolved stars. The best fit straight line is drawn through the data points (dot-dashed line). b) The same, for the 547-814 color.
- Fig. 6.— a) and b) as in Figure 5, now for the 8 regions selected inside and around the E–W dust lane. The two straight lines represent: the foreground dust layer (dotted line) and the 'effective reddening' curve derived from Equation (3) (continuous line). The curved line represents the 'sandwich' dust model (dot-dashed line.
- Fig. 7.— Color-Color plot of the inner $16'' \times 16''$. Each data point corresponds to a bin 0'.5 in size. The colors 255-547 and 547-814 are in the STMAG system. The straight line at the bottom left corner is the reddening vector for $A_V=1$ mag. The error bar at the top right corner shows the uncertainty given by the photon statistics of a 6 σ detection, convolved with the photometric uncertainties. The vast majority of the data points in the plot have detection level higher than 6 σ .
- Fig. 8.— a) As in Figure 7, after correction for dust reddening applying the observed mean

obscuration (Equation (3) and (1)). The error bar at the upper right corner of the figure is as in Figure 5. The continuous line marks the evolutionary sequence for the colors of a stellar population with constant star formation, in the age range 1 Myr–15 Gyr; the filled triangles mark a set of relevant ages in this sequence: 1, 3, 5, 8, 10, 20, 50, 100, 200, 500, 1000, 5000, and 15000 Myr. b) and c) The colors of the inner $16'' \times 16''$ are plotted as a function of the H α line equivalent width after reddening correction (see text). The 1 σ uncertainty is shown in the top left corner of each diagram. The colors are the b) 255–547 and c) 547–814. The continuous line marks the evolutionary sequence of a stellar population with constant star formation, in the age range 1–500 Myr (LH95); the filled triangles have the same age separation as panel a).

Fig. 9.— Color-color plot of a 5".5×5".5 region of the galaxy centered on the H α emission peak, at the position of the starburst nucleus. Each data point is a 0".5 square bin. The surface brightness of each bin has been galaxy-background subtracted; the background has been derived from an annulus of 3" inner radius, and 2" thickness. Only points with fluxes at least 2 σ above the defined background have been reported in the plot. The data are corrected for dust reddening following Equations (1) and (3). The continuous line corresponds to continuous star formation at the different age values indicated in the figure. The dot-dash line corresponds to an instantaneous burst population in the age range 1–100 Myr (from the bluest to the reddest 255–547 point); the 'knee' at 547–814 \simeq –0.4 marks an age of about 10 Myr (Bruzual & Charlot 1995).



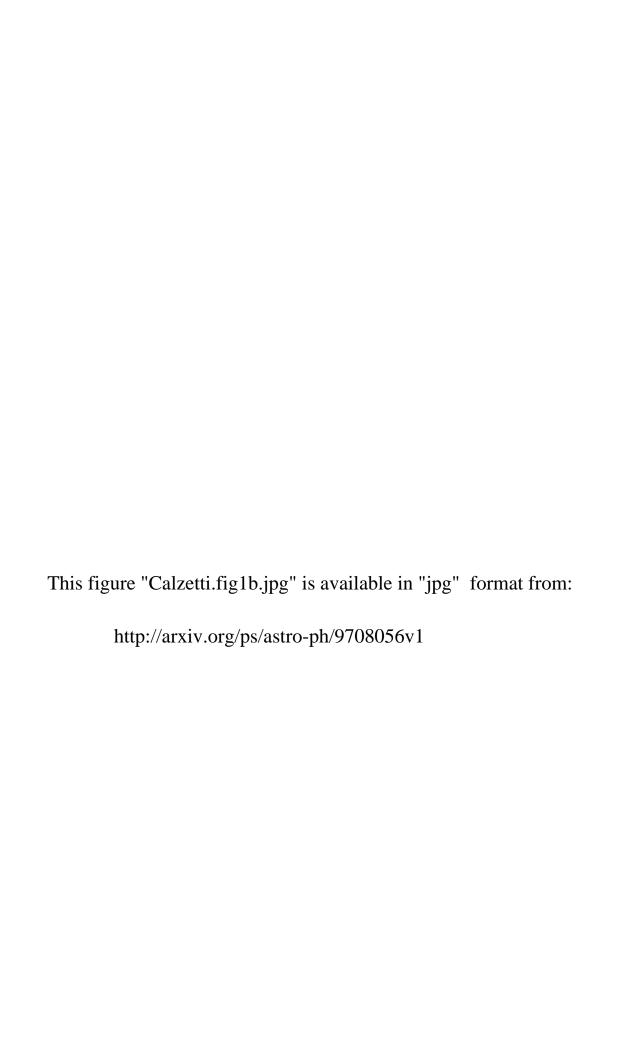


TABLE 1Log of the Exposures

Exposure Name	Filter	Mean Wavelength (Å)	Filter Bandpass (Å)	Exposure Time (sec)	Shift ^a (pixels)
U3760101	F487N	4865.	25.8	1200.	(0,0)
U3760102	F487N	4865.	25.8	1300.	(0,0)
U376010F	F487N	4865.	25.8	1300.	(5,5)
U376010G	${ m F487N}$	4865.	25.8	1300.	(5,5)
U3760107	F547M	5484.	483.1	200.	(0,0)
U3760108	F547M	5484.	483.1	600.	(0,0)
U3760109	F547M	5484.	483.1	200 .	(5,5)
U376010A	F547M	5484.	483.1	600.	(5,5)
U3760103	F656N	6564.	21.4	500 .	(0,0)
U3760104	F656N	6564.	21.4	1500.	(0,0)
U376010D	F656N	6564.	21.4	500 .	$(5,\!5)$
U376010E	F656N	6564.	21.4	1100.	$(5,\!5)$
U3760105	F814W	7921.	1488.8	400.	(0,0)
U3760106	F814W	7921.	1488.8	180.	(0,0)
U376010B	F814W	7921.	1488.8	180.	(5,5)
U376010C	F814W	7921.	1488.8	400.	(5,5)
$\rm U2P00101^{b}$	F225W	2586.	393.2	700.	(0,0)
U2P00102	F225W	2586.	393.2	700.	(0,0)
U2P00103	F225W	2586.	393.2	700.	(0,0)
U2P00104	F225W	2586.	393.2	800.	(-5,5)
U2P00105	F225W	2586.	393.2	800.	(-5,5)
U2P00106	F225W	2586.	393.2	800.	(-5,5)
U2P00107	F225W	2586.	393.2	800.	(5,5)
U2P00108	F225W	2586.	393.2	800.	(5,5)
U2P00109	F225W	2586.	393.2	800.	(5,5)

^aShift relative to the nominal telescope pointing, $\alpha(\text{J}2000) = 13:39:56.0, \delta(\text{J}2000) = -31:38:26$ in the aperture WF3-FIX. $$^{\rm b}{\rm The~exposures}$ in the F225W filter are from HST archival data.

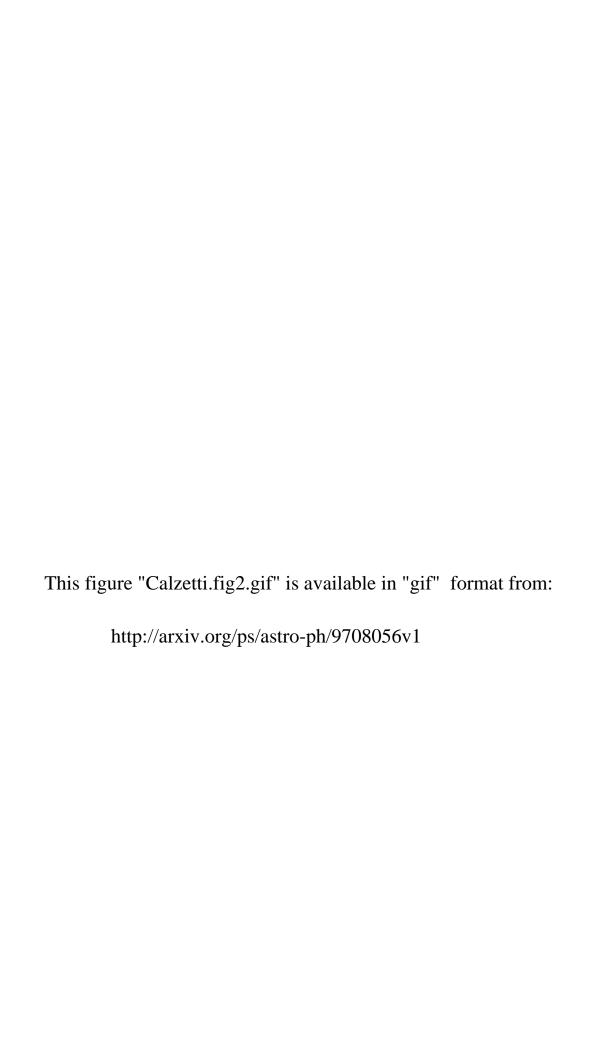


TABLE 2 PHOTOMETRIC COMPARISON: IMAGE-SPECTRUM

Filter	WFPC2 Flux Density ^a (erg s ⁻¹ cm ⁻² Å ⁻¹)	WFPC2 Detection Limit ^b (erg s ⁻¹ cm ⁻² pix ⁻¹)	Spectrum Flux Density ^c (erg s ⁻¹ cm ⁻² Å ⁻¹)
F225W	$(7.18\pm0.36) \text{ E}{-14}$	11.35 E-19	$6.72 E{-}14$
F547M	$(2.41\pm0.12) \text{ E}{-14}$	$1.35 \text{ E}{-}19$	$2.44 \; \mathrm{E}{-14}$
F814W	$(1.37\pm0.10) E-14$	$1.13 \text{ E}{-19}$	$1.41 \; \mathrm{E}{-14}$
${ m F487N^d}$	$(2.60\pm0.23) E-14$		$2.72 \; \mathrm{E}{-14}$
${ m F656N^d}$	$(2.01\pm0.17) \text{ E}{-14}$		$1.90 \; \mathrm{E}{-14}$
${ m F487N^e}$	$(2.35\pm0.07) \text{ E}{-12}$	$9.42 \ \mathrm{E}{-19}$	$2.42 \; \mathrm{E}{-12}$
${ m F656N^e}$	$(8.01\pm0.24)\ E{-}12$	$6.01 \; \mathrm{E}{-19}$	$8.00 \; \mathrm{E}{-12}$

^aFlux densities from the WFPC2 images are extracted from apertures which match those of the IUE/ground-based ultraviolet and optical spectrum. Uncertainties combine background subtraction, calibration uncertainty and continuum/emission line subtraction (where necessary, see text).

^bThe 5 σ detection limits in the WFPC2 filters. ^cFlux densities are derived after convolution of the spectrum with the WFPC2 filter bandpasses, using the STSDAS Synphot package.

^dThe quoted flux densities are for the stellar continuum only, after removal of the contribution from the ionized gas.

^eEmission line fluxes, in units of erg s⁻¹cm⁻², for the H β (F487N) and the [NII] $(6548 \text{ Å}) + \text{H}\alpha \text{ (F656N)}$, respectively.

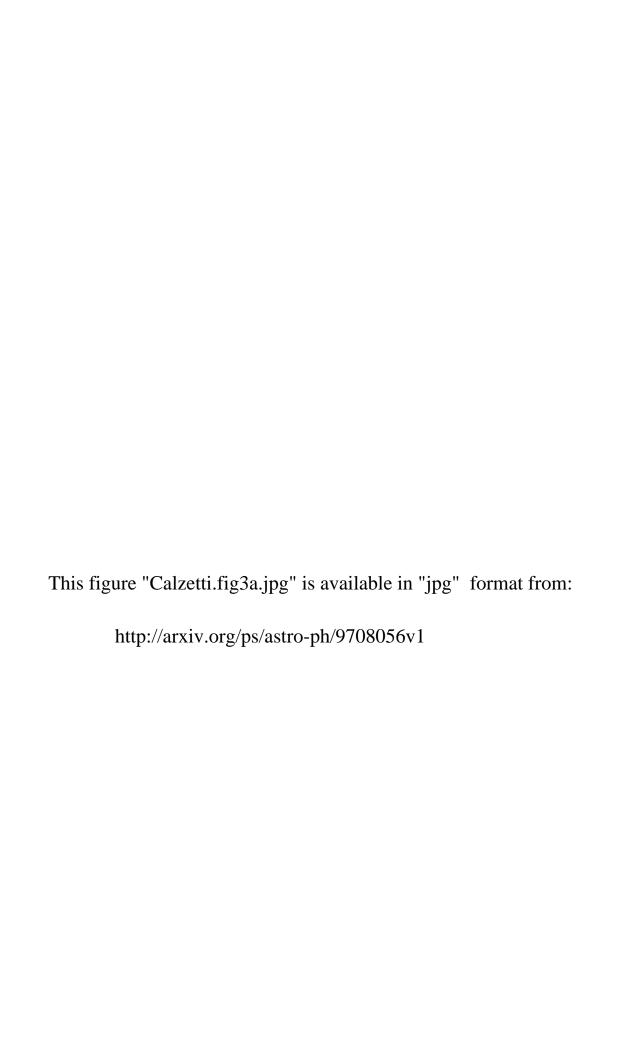




TABLE 3
ASTROMETRY AND PHOTOMETRY OF THE CLUSTERS

${ m ID^a}$	$\alpha(2000)$	$\delta(2000)$	${ m A}_{etalpha}{}^{ m b}$	${{ m m}_{547}}^{ m d} \ m (STMAG)$	$255-547^{\rm d}$ (STMAG)	$547-814^{\rm d}$ (STMAG)	$F(H\alpha)$ (erg s ⁻¹ cm ⁻²)	$\mathrm{EW}(\mathrm{H}lpha)^{\mathrm{e}} \ (\mathrm{\mathring{A}})$	$\mathrm{EW}(\mathrm{H}eta)^{\mathrm{e}} \ (\mathrm{\mathring{A}})$	${ m Age} \ 10^6 { m yr}$
NGC5253-1 (UV-2)	13:39:55.988	-31:38:31.85		17.34	-1.62	-0.36	1.91E-15	5	1	
			0.00	17.19	-1.80	-0.42	2.14E-15	5	1	8 - 12
NGC5253-2 (UV-4)	13:39:55.586	-31:38:29.31		17.46	-0.77	-0.48	1.00E - 15	3	<1	
			~ 0.00	17.31	-0.96	-0.54	1.12E-15	~5	<3	50 - 60
NGC5253-3	13:39:55.536	-31:38:29.73		17.51	-0.94	-0.29	1.44E - 15	4	1	
			~ 0.00	17.36	-1.13	-0.35	1.61E-15	~6	∼ 3	30 - 50
NGC5253-4 (UV-1)	13:39:55.936	-31:38:27.52		17.58	-2.10	-0.97	$1.17\mathrm{E}\!-\!13$	434	86	
			0.14	17.16, 17.06	-2.47, -2.71	-1.10, -1.18	1.71E-13	457	97	2.5 - 4.4
NGC5253-5 (UV-12)	13:39:56.007	-31:38:25.00		17.87	-1.26	+0.00	4.76 E - 13	1650	427	
			0.35	17.04, 16.80	-1.91, -2.52	-0.23, -0.47	> 1.05 E-12	1878	574	2.2 - 2.8
			c	~ 15	-2.35, -2.60	-0.66, -0.76	$6.02 ext{E-}12, 7.04 ext{E-}12$	1650	427	02.8
NGC5253-6	13:39:55.373	-31:38:33.92		18.13	-1.43	-0.54	$3.26 E\!-\!15$	18	6	
			0.00	17.97	-1.61	-0.60	3.65 E-15	18	6	10 - 17

^aThe clusters are listed in order of decreasing *observed* brightness in the V band (first row for each cluster). In parenthesis, the identification of Meurer et al. 1995, based on the UV brightness, is given.

^eThe first row for each cluster reports the observed EWs. The subsequent rows give the EWs corrected for differential reddening between gas emission and stellar continuum (see text).

^bMagnitudes of foreground attenuation between Hα and Hβ, after removal of the extinction from our Galaxy (E(B-V)=0.05), and after correcting the nebular emission for the effects of the underlying stellar absorption, $EW_{abs}(H\alpha)=EW_{abs}(H\beta)=2$ Å. NGC5253-1 and NGC5253-6 have zero intrinsic extinction, $A_{\beta\alpha}=0$, already after correction for the small foreground extinction from our Galaxy. For NGC5253-2 and NGC5253-3, the correction for the underlying stellar absorption changes the intrinsic reddening from $A_{\beta\alpha}=0.22$ and $A_{\beta\alpha}=0.15$, respectively, to $A_{\beta\alpha}\sim0$.

^cPhotometry of NGC5253-5, after the reddening correction is performed assuming that the cluster is embedded in a homegeneous dust cloud with 9 mag of optical depth, and is behind foreground dust with A_V =0.30 (first set of numbers in each column) and 0.45 (second set of numbers), respectively. The uncertainty in the colors is about $\delta(255-547)$ =0.35 and $\delta(547-814)$ =0.13.

^dPhotometry and colors of the clusters. For each cluster, the first line gives the measured values, the subsequent lines the reddening corrected values. For NGC5253-4 and NGC5253-5, columns 5, 6, 7 can be double valued: the first set of numbers are the V magnitude and the colors, respectively, after correction for the observed mean reddening of the stellar continuum (Equation (3)); the second set of numbers are after correction for pure foreground dust. This does not apply to the third row of NGC5253-5 (see Note c). Uncertainties in the magnitudes due to aperture effects are $\delta m \simeq 0.15-0.30$; uncertainties in the colors are $\delta (255-547) \simeq \pm 0.07$ and $\delta (547-814) \simeq \pm 0.06$.

